Available online at www.sciencedirect.com
SCIENCE DIRECT
Journal of the European Ceramic Society 26 (2006) 875–882
www.elsevier.com/locate/jeurceramsoc

Structural determination and microwave properties of $(x)Re(Co_{1/2}Ti_{1/2})O_3–(1-x)CaTiO_3$ (Re = La and Nd) solid solutions

D.L. Cairns [a,*], I.M. Reaney [a], N. Otten [a], D. Iddles [b], T. Price [b]

[a] *Department of Engineering Materials, Sir Robert Hadfield Building, Mappin Street, Sheffield S1 3JD, UK*
[b] *Filtronic Comtek, Enterprise Drive, Station Road, Four Ashes, Wolverhampton, WV10 7DB, UK*

Received 10 September 2004; received in revised form 18 November 2004; accepted 26 November 2004
Available online 3 February 2005

Abstract

Solid solutions of $(x)Re(Co_{1/2}Ti_{1/2})O_3–(1-x)CaTiO_3$ (Re = La and Nd, abbreviated to *x*LCT and *x*NCT, respectively) where $x = 0$, 0.25, 0.5, 0.75 and 1 have been fabricated using solid state synthesis. Samples have been examined using X-ray diffraction (XRD), scanning electron microscopy, transmission electron microscopy (TEM) and their dielectric properties measured at microwave (MW) frequencies. Formation of single phase solid solutions were confirmed by XRD and the measured lattice parameters varied linearly from LCT ($a = 5.66$ Å, $b = 7.867$ Å and $c = 5.494$ Å) and NCT ($a = 5.636$ Å, $b = 7.914$ Å and $c = 5.461$ Å) to CT ($a = 5.596$ Å, $b = 7.731$ Å and $c = 5.424$ Å). XRD and TEM confirmed both in-phase and antiphase rotations of O-octahedra consistent with an $a^-a^-c^+$ tilt system across the entire solid solution series. Electron diffraction revealed that LCT and NCT have reflections associated with B-site cation ordering which is absent for $x \leq 0.75$. MW dielectric measurements showed that LCT and NCT were highly insulating with microwave quality factor (Qf_0) values of 39,000 and 34,000, respectively. Compositions anticipated to have a zero temperature coefficient of resonant frequency (τ_f) are 0.48LCT-CT and 0.52NCT-CT with $\varepsilon_r = 45$ and $Qf_0 \sim 5000$ and $\varepsilon_r = 43$ and $Qf_0 \sim 4000$, respectively.

Keywords: La(Co,Ti)O_3; Dielectric properties; Microwave dielectrics; $CaTiO_3$

1. Introduction

Candidate materials for MW dielectric resonators suitable for 3G technology must satisfy three main criteria; high quality factor ($Q > 15{,}000$), permittivity, $\varepsilon_r > 25$ and a temperature coefficient of resonant frequency, $\tau_f = \pm 3$ ppm/°C. Q is defined as the resonant frequency (f_0) divided by the bandwidth (Δf_0) at 3 dB below peak height, shown in Eq. (1):

$$Q = \frac{f_0}{\Delta f_0} \tag{1}$$

The Q value ($Q = 1/\tan\delta$) is a measure of a resonating body's ability to resonate at a given frequency. A Qf_0 value is usually quoted which is a figure of merit to compare resonating bodies of different sizes and permittivities. ε_r is related to f_0 and the volume, V, of the resonating disc as shown by Eq. (2).

$$f_0 \propto \frac{1}{V\sqrt{\varepsilon_r}} \tag{2}$$

The final parameter is the temperature coefficient of resonant frequency (τ_f) which should be tunable through zero to stop drift of the resonant frequency with temperature and is given by Eq. (3).

$$\tau_f = -\left(\frac{1}{2}\tau_\varepsilon + \alpha_L\right) \tag{3}$$

where τ_ε is the temperature coefficient of relative permittivity and α_L the linear thermal expansion coefficient.

In 1994, a patent emerged from the Kyocera Corporation detailing a new zero τ_f material $0.65CaTiO_3–0.35NdAlO_3$ (0.65CT-NA).[1] This material replaced existing dielectric

* Corresponding author.
E-mail address: mtq01dc@sheffield.ac.uk (D.L. Cairns).

0955-2219/$ – see front matter © 2004 Elsevier Ltd. All rights reserved.
doi:10.1016/j.jeurceramsoc.2004.11.024

resonators such as Sn-doped zirconium titanate (ZTS) due to its superior properties, $\varepsilon_r = 45$ and $Qf_0 \sim 43{,}000$. Zero τ_f was achieved by producing a composition in a solid solution formed from positive (CT, $\varepsilon_r = 160$, $Qf_0 = 12{,}000$ GHz and $\tau_f = +850\ MK^{-1}$) and negative τ_f ($NdAlO_3$, $\varepsilon_r = 20$, $Qf = 50{,}000$ GHz and $\tau_f = -33\ MK^{-1}$) end members.[2] Since the emergence of this compound several researchers have attempted to form similar solid solutions with CT using different negative τ_f lanthanide based perovskite end members, e.g., $La(Mg_{1/2}Ti_{1/2})O_3$ (LMT, $\varepsilon_r = 27.6$, $Qf_0 = 70{,}000$ and $\tau_f = -81\ MK^{-1}$) and $Nd(Mg_{1/2}Ti_{1/2})O_3$ (NMT, $\varepsilon_r = 25.9$, $Qf \sim 60{,}000$ and $\tau_f = -47\ MK^{-1}$).[3]

At room temperature LMT and NMT have a distorted perovskite structure due the occurrence on cooling of a sequence of structural phase transitions, which involve rotations of the oxygen octahedral (Glazer tilt system, $a^-a^-c^+$).[4] In addition, X-ray and electron diffraction data have shown that LMT and NMT have 1:1 ordered B-site ions in a generic 'rock salt' arrangement which in combination with the $a^-a^-c^+$ tilt system results in a monoclinic $P2_1/n$ space group.[5] At room temperature, CT has the same tilt system, $a^-a^-c^+$, as LMT and NMT but clearly no B-site ordering is possible and the space group remains that defined uniquely by the oxygen octahedral tilt system, *Pbnm*. It has generally been observed that the addition of CT to the LMT and NMT end members destroys B-site ordering. In both CT-LMT and CT-NMT systems zero τ_f occurs at $x \sim 0.5$ which gives a reduction in Qf_0 values, from the LMT and NMT end members, due to the loss of B-site cation ordering.[6–8]

The substitution of Co^{2+} for Zn^{2+} in $Ba([Co_xZn_{1-x}]_{1/3}Nb_{2/3})O_3$ (BCZN) has been shown to tune τ_f close to zero. It has also been shown that co-doping with 10 at.% Ga^{3+}/Ta^{5+} on the B-site results in a high Qf_0 (32,000 @ 2.8 GHz) composition, $0.9Ba([Co_{0.40}Zn_{0.60}]_{1/3}Nb_{2/3})O_3$–$0.1Ba(Ga_{1/2}Ta_{1/2})O_3$ (BCZN-BGT).[9] Co is a transition metal and as such has a variable oxidation state between 2 and 4. BCZN has an ordered $2\ Nb^{5+}$:Co^{2+}, B-site trigonal superlattice and, is therefore, stoichiometric.[10] However, very little is known about compounds where Co ions share the B-site with, e.g., Ti^{4+}, whose valence state may also vary depending on process conditions. Recently, $La(Co_{1/2}Ti_{1/2})O_3$ (LCT) has been fabricated to give a highly insulating material with $\varepsilon_r = 25$, $Qf_0 \sim 39{,}000$ and TCF = $-42\ MK^{-1}$.[11] These values suggest that LCT and possibly the sister compound $Nd(Co_{1/2}Ti_{1/2})O_3$ (NCT) may be suitable as end-members in solid solution with $CaTiO_3$. Therefore, it is the intention of this paper to investigate the microstructure and structure of ${}_xLCT\text{-}_{1-x}CT$ and ${}_xNCT\text{-}_{1-x}CT$ solid solutions and assess their suitability as temperature-stable MW dielectric ceramics.

2. Experimental

All solid solutions, general formulae ${}_xLa(Co_{1/2}Ti_{1/2})O_{3-(1-x)}CaTiO_3$ (xLCT) and ${}_xNd(Co_{1/2}Ti_{1/2})O_{3-(1-x)}CaTiO_3$ (xNCT), were synthesised using a conventional mixed oxide route with raw materials of La_2O_3, Nd_2O_3, TiO_2, $CoCO_3$ and $CaCO_3$ (Acros Organics, >99%). The starting reagents, weighed in the appropriate ratios, were balled milled for 16 h in propan-2-ol using ZrO_2 media. All pre-reacted powders had a mean particle diameter of 1 μm, Laser Coulter Analyser. The slurry was dried at 100 °C then calcined at 1350 °C for 6 h, $CaTiO_3$ was calcined at 1150 °C for 4 h. The calcined powders were re-milled for 16 h in propan-2-ol. The dried powders were pressed into 1 and 2 cm discs and sintered at 1550 °C for 6 h on ZrO_2 boards, $CaTiO_3$ was sintered at 1600 °C for 4 h. Densities were calculated using the Archimedes water method and all sintered discs had a density of >96% of theoretical.

An X-ray diffractometer (Model PW 1730/10 Philips, Holland) with Cu Kα source (λ = 1.540562 Å), operated at 50 kV and 30 mA, was used for the identification of phases in the calcined powders and sintered pellets. A step size of 0.02°, a scan rate of 2°/min and scan ranges of 10–70° were adopted. Samples for scanning electron microscopy (SEM) were obtained from fracture surfaces of the sintered pellets. Samples were then mounted on stainless steel stubs using silver dag and carbon coated. A JEOL JSM6400 SEM equipped with a LINK energy dispersive spectroscopy (EDS) detec-

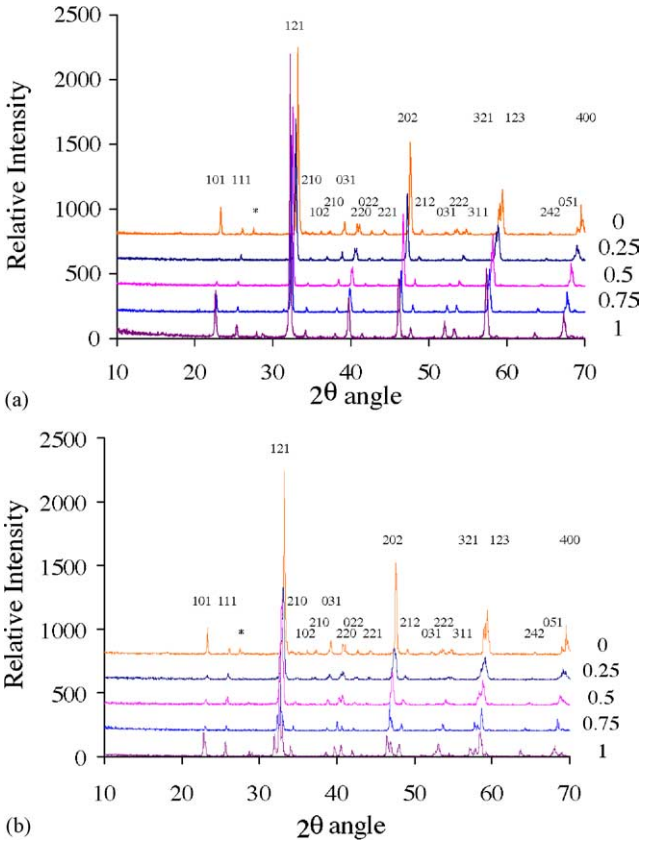

Fig. 1. XRD traces from the (a) xLCT and (b) xNCT solid solution series indexed using an orthorhombic setting.

tor and ancillary electronics operating at 20 kV was used to obtain secondary electron images. Samples for transmission electron microscopy (TEM) were ground to approximately 30 μm thick after which a Cu support ring with an 800 μm circular hole was glued onto its surface. Samples were then thinned on a Gatan Duo Mill ion beam thinner operating at an accelerating voltage of 6 kV and a combined gun current of 0.6 mA at an incidence angle of 15°. TEM was carried out on a Phillips EM420 operating at 120 kV.

The microwave dielectric properties were calculated using 2 cm pellets. Microwave measurements (ε_r, Q and τ_f) were performed using a silver plated aluminium cavity >∼4 times the diameter of the test resonator (this ensured an "isolated" but shielded resonator) and an Agilent vector network analyser (8753ES) with a range from 30 kHz to 6 GHz. Samples were located at the centre of the cavity on a 99.5% alumina support, thus avoiding any influence from the metallic cavity walls. Microwave energy was coupled to the test piece using a single probe, measuring in reflectance. After calibration for the cables and cavity, the coupling was adjusted such that losses were lower than −30 dB. Q is approximated using Eq. (4):

$$Q = \frac{f_0}{\mathrm{BW}} \tag{4}$$

where f_0 is the resonant frequency and BW is the bandwidth measured using the full-width half-maximum value from the resonant peak. Measurement of Q was at ambient temperature and the resonance mode measured was $TE_{01\delta}$. τ_f measurements were performed in the same aluminium cavity placed inside a Tenney temperature control cabinet. Resonant frequency measurements were performed at 60, 20 and −10 °C when the $TE_{01\delta}$ mode was stable.

3. Results and discussion

3.1. X-ray diffraction

Fig. 1 shows the X-ray diffraction (XRD) traces from compositions in the *x*LCT and *x*NCT solid solution series. Compounds in these solid solutions have hitherto not been fabricated, and therefore, no JCPDS data files were available to match with the experimental traces. Instead, peaks were indexed according to either $CaTiO_3$ (JCPDS 42–423, *Pbnm*) for compositions were $x < 1$ and LMT (JCPDS 49-242, $P2_1/n$) or $Nd(Mg_{1/2}Ti_{1/2})O_3$ (NMT) for $x = 1$ (JCPDS 77–2426, $P2_1/n$). Two unidentified peaks occurred at the same 2θ values on each trace. These peaks could be indexed according to monoclinic ZrO_2 (JCPDS 42-1146), which is used as the milling media and could arise as a contami-

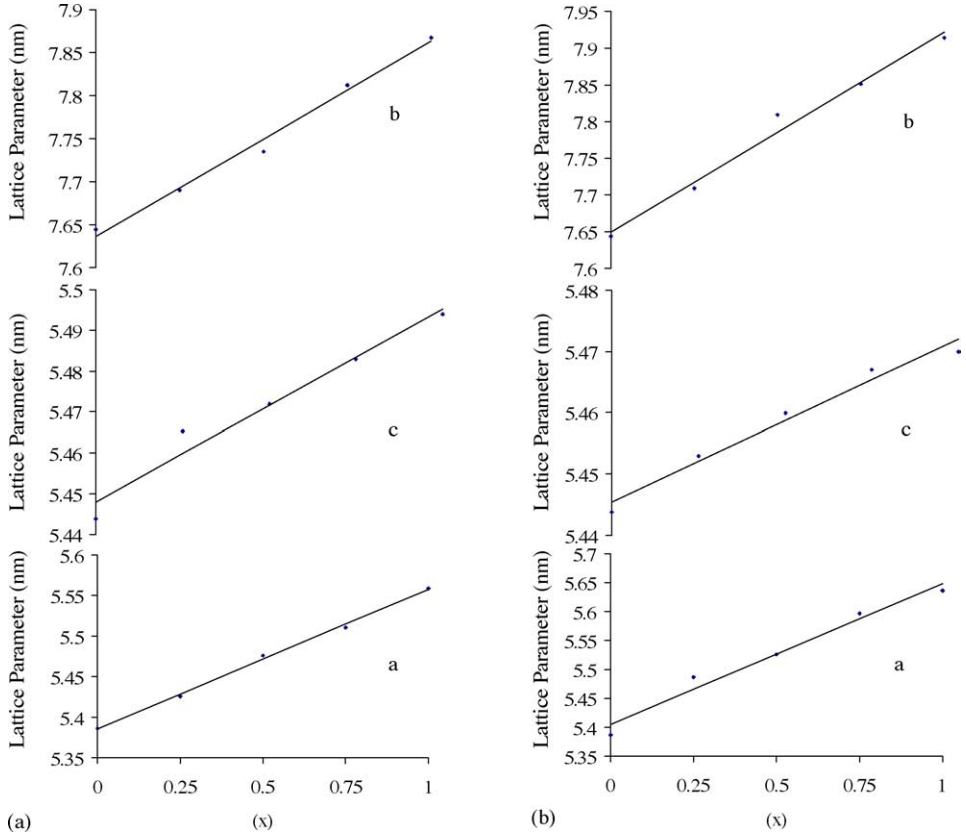

Fig. 2. Lattice parameter measurements from (a) LCT-CT and (b) NCT-CT solid solutions.

nant. All compositions are indexed according to either an orthorhombic (*Pnma*) or pseudo-orthorhombic ($P2_1/n$) cell unit in which the Glazer tilt system,[4] $a^-a^-c^+$, tilt describes the distortions of the O-octahedra. The lattice parameters varied linearly from LCT ($a = 5.66$ Å, $b = 7.867$ Å and $c = 5.494$ Å) and NCT ($a = 5.636$ Å, $b = 7.914$ Å and $c = 5.461$ Å) to CT ($a = 5.596$ Å and $b = 7.731$ Å, $c = 5.424$ Å) confirming the formation of a solid solution, shown in Fig. 2. Superlattice reflections due to the $a^-a^-c^+$ tilt system arise at $\frac{1}{2}$ integer positions in a pseudocubic (p) perovskite setting. In addition, however, in LMT and NMT, the B-site ions are ordered to form a generic rock salt superlattice which gives rise to unique reflections at $\frac{1}{2}\{\mathrm{o\,o\,o}\}_\mathrm{p}$, $h = k = l$ positions (o, odd and e, even). These reflections are weak for LMT and NMT but absent in the LCT and NCT traces shown in Fig. 1. The scattering length difference between Co^{2+} and Ti^{4+} is, however, smaller than that between Mg^{2+} and Ti^{4+} and ordering peaks may be difficult to resolve by XRD.

3.2. SEM results

Fig. 3 shows secondary electron SEM images obtained from NCT, LCT 0.5LCT, 0.5NCT and CT compositions. All images show microstructures with little porosity consistent with a measured density of >95% theoretical. Grain sizes vary from 1 to 5 μm for the *x*LCT series and 5 to 10 μm for the *x*NCT solid solution. Energy dispersive spectroscopy (EDS) and backscattered electron imaging revealed no second phases with only the expected elements in the appropriate ratios.

3.3. TEM results

Fig. 4 shows typical ferroeleastic domain structures in LCT, NCT and CT end members which are present in all compositions across the solid solution series due to structural phase transitions involving rotations of the O-octahedra to give an $a^-a^-c^+$ tilt system. As discussed in Section 3.1, the $a^-a^-c^+$ tilt system gives rise to reflections at $\frac{1}{2}$ integer pseudocubic positions. Fig. 5 shows the $\langle 1\,1\,0\rangle_\mathrm{p}$ and $\langle 1\,1\,1\rangle_\mathrm{p}$ zone axis diffraction patterns (ZADPs) from NCT and 0.5NCT. Identical patterns were obtained from LCT and 0.5LCT. The fundamental spots (strong) are indexed according to a pseudocubic perovskite cell and superlattice reflections are present in all patterns at half-integer positions. In general, $\frac{1}{2}\{\mathrm{o\,o\,o}\}_\mathrm{p}$ (arrowed) arise either from rotations of

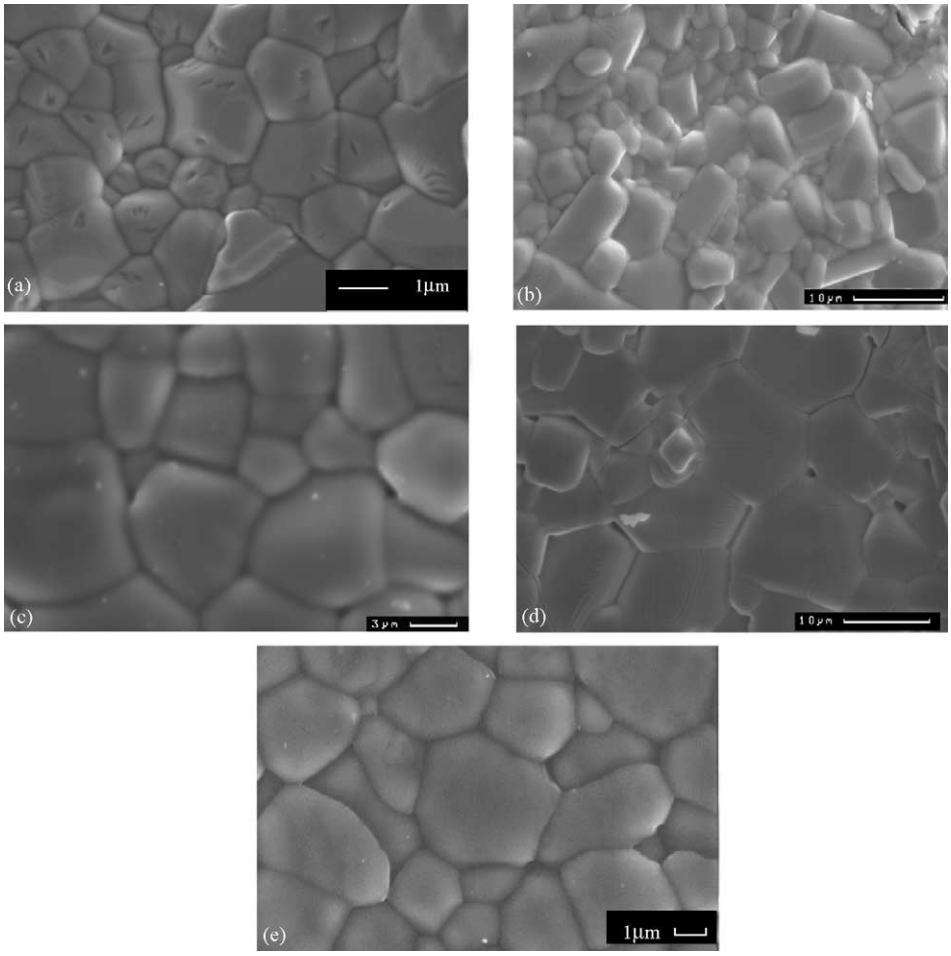

Fig. 3. Secondary electron SEM images from (a) LCT, (b) NCT, (c) 0.5LCT, (d) 0.5NCT and (e) CT.

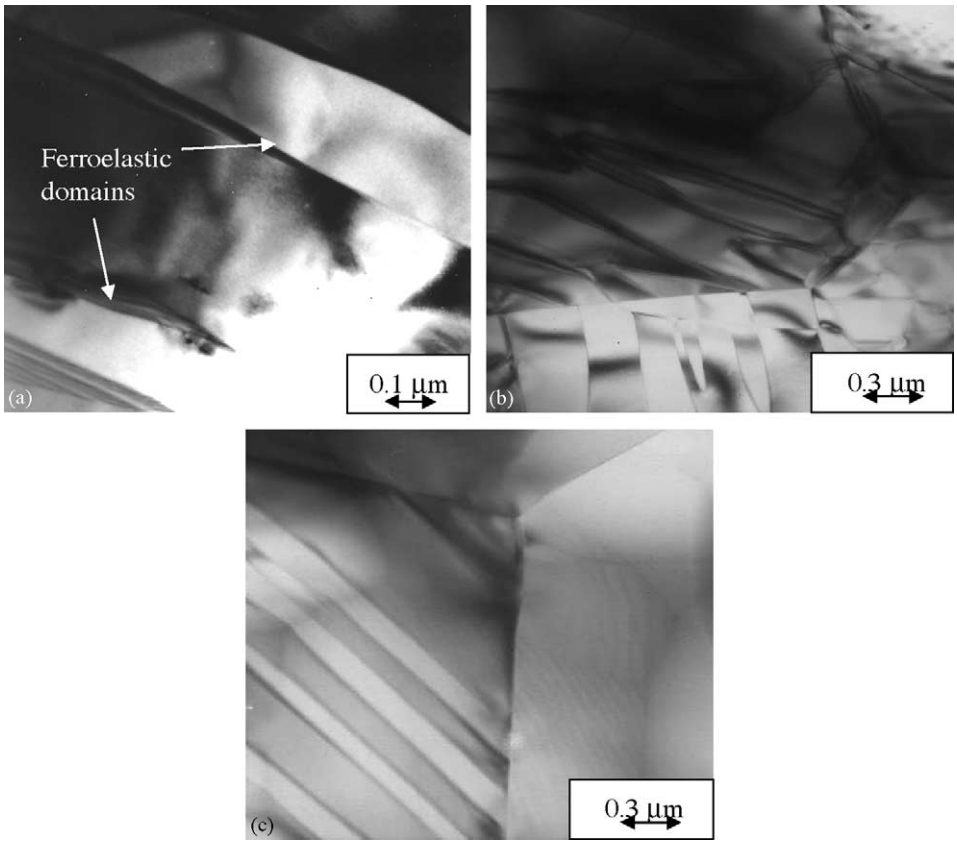

Fig. 4. Bright field TEM images showing typical ferroelastic domains from (a) NCT, (b) LCT and (c) CT.

the o-octahedra in anti-phase or rocksalt ordering of the Co and Ti ions, $\frac{1}{2}\{o\,o\,e\}_p$ (square) arise from in-phase rotations of the o-octahedra and $\frac{1}{2}\{o\,e\,e\}_p$ (circled) arise from antiparallel cation displacements.[12] All reflections in all zones are consistent with an $a^-a^-c^+$ tilt system which gives rise to either a *Pbnm* (disordered Co/Ti ions) or $P2_1/n$ (ordered) space group[4] but, according to computer simulations and using the reflection conditions for *Pbnm* ($a^-a^-c^+$), the $[1\text{–}10]_p$ variant for NCT (Fig. 5a) should not contain $\frac{1}{2}\{o\,o\,o\}_p$ reflections associated with anti-phase rotations of the O octahedra. The presence of these reflections, therefore, suggests that the Co and Ti ions in NCT are ordered in a similar manner to that reported in LMT and NMT, consistent with space group $P2_1/n$. In contrast, the $\frac{1}{2}\{o\,o\,o\}_p$ reflections in the $[1\text{–}10]_p$ variant are absent for xNCT, $x<1$, as typified by 0.5NCT, Fig. 5b. This is consistent with the disruption of B-site cation ordering as the Co:Ti ratio deviates from 1:1. Figs. 5c and d are $[1\,1\,0]_p$ variants from NCT and 0.5NCT in which the $\frac{1}{2}\{h\,k\,l\}_p$ superlattice reflections may arise from either anti-phase rotations or ordering and as a result cannot be used to distinguish $P2_1/n$ from *Pbnm* symmetry.

In Fig. 5a, $\frac{1}{2}\{o\,o\,e\}$ ($h=k$) reflections are also present. These are forbidden according to the selection rules for *Pbnm* and $P2_1/n$ but may arise by the generic double diffraction route as shown in Eq. (5);

$$\tfrac{1}{2}\{o\,o\,o\} + \tfrac{1}{2}\{e\,e\,o\} = \tfrac{1}{2}\{o\,o\,e\} \quad (5)$$

The ⟨1 1 1⟩ ZADP's are consistent with both *Pbnm* and $P2_1/n$ symmetry and, are therefore, identical for NCT (Fig. 5e) and 0.5NCT (Fig. 5f). The Weiss zone law forbids reflection of the type $\frac{1}{2}\{o\,o\,o\}_p$ (antiphase tilting/1:1 ordering) in $\langle 1\,1\,1\rangle_p$ ZADP's but allows $\frac{1}{2}\{o\,o\,e\}_p$ which arise only from in-phase tilting. Identical trends are observed in the electron diffraction data the xLCT solid solution series.

3.4. Microwave dielectric properties

Fig. 6a and b show the variation in Qf_0 across the xLCT and xNCT solid solution series, respectively. Although the initial values of Qf_0 for $x=1$ are high (>35,000) for both solid solutions, there is a steep decrease as the CT concentration increases. This is attributed to the loss of long range B-site ordering,[13] present for $x=1$ but absent for $x<1$, as observed by electron diffraction. Fig. 6c and d are plots of τ_f and ε_r versus x for xLCT and xNCT, respectively. For both compositional series, the permittivity increases from 28 (LCT) and 26 (NCT) to ∼160 as x varies from 1 to 0, respectively. This is accompanied by an increase in τ_f from

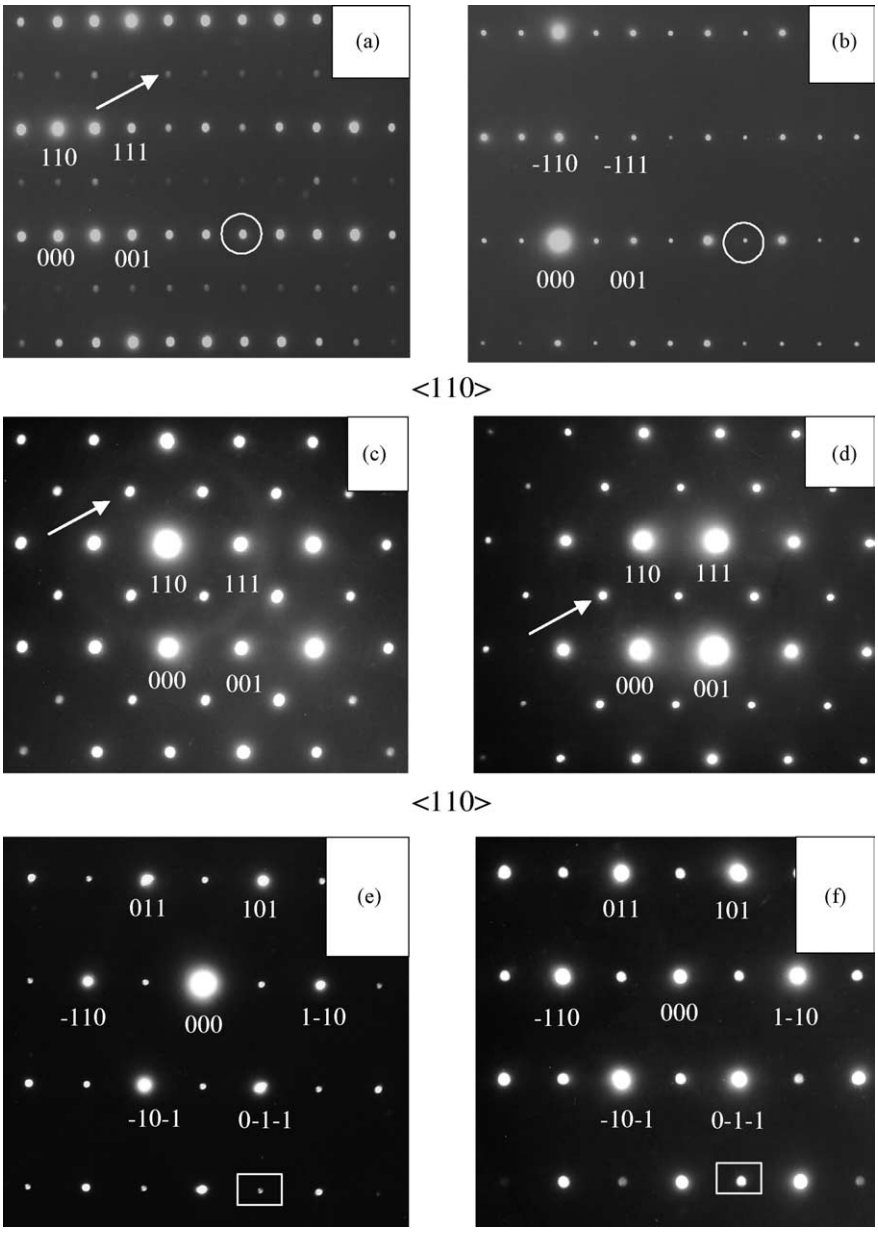

Fig. 5. Selected area diffraction patterns with the electron beam parallel to the (a), (b), (c) and (d) $\langle 1\,1\,0\rangle_p$ and (d) and (e) $\langle 1\,1\,1\rangle_p$ pseudocubic axes of grains in NCT and 0.5NCT compositions.

−36 ppm/°C and −58 ppm/°C to +800 ppm/°C. Moreover, when ε_r is plotted against τ_f, the relationship is linear over the broad range of values for each series, Fig. 7. LCT, NCT and CT have the same Glazer tilt system ($a^-a^-c^+$) which is retained across the solid solution series. Therefore, apart from the loss of B site order for $x < 1$ there are no structural phase transitions as a function of x. Harrop[14] predicted and demonstrated empirically that over a broad range, $\varepsilon_r \propto -\tau_\varepsilon$ for dielectric materials. Therefore, neglecting α_L (typically 10–15 ppm/°C for perovskites), it follows that ε_r is also directly proportional to τ_f since $\tau_f \propto -\tau_\varepsilon$. This relationship has been confirmed for perovskites and related materials by Wise et al.[15] and by Seabra et al.[16] Deviations from this relationship only occur in solid solutions when there is a displacive phase transition as x increases, e.g., octahedral tilt transitions (Reaney et al.[12] and Colla et al.[17]). Since xLCT and xNCT solid solutions remain distorted with the same Glazer tilt system across the solid solution series, a linear relationship between ε_r and τ_f is expected. Estimated dielectric properties at the zero τ_f compositions are $\varepsilon_r \sim 45$ and $Qf_0 \sim 5000$ (xLCT) and $\varepsilon_r \sim 43$ and $Qf_0 \sim 4000$ x(NCT). The permittivities are comparable with commercial ceramics, e.g., $CaTiO_3$–$NdAlO_3$, but currently the Qf_0 values are too low for commercial exploitation.

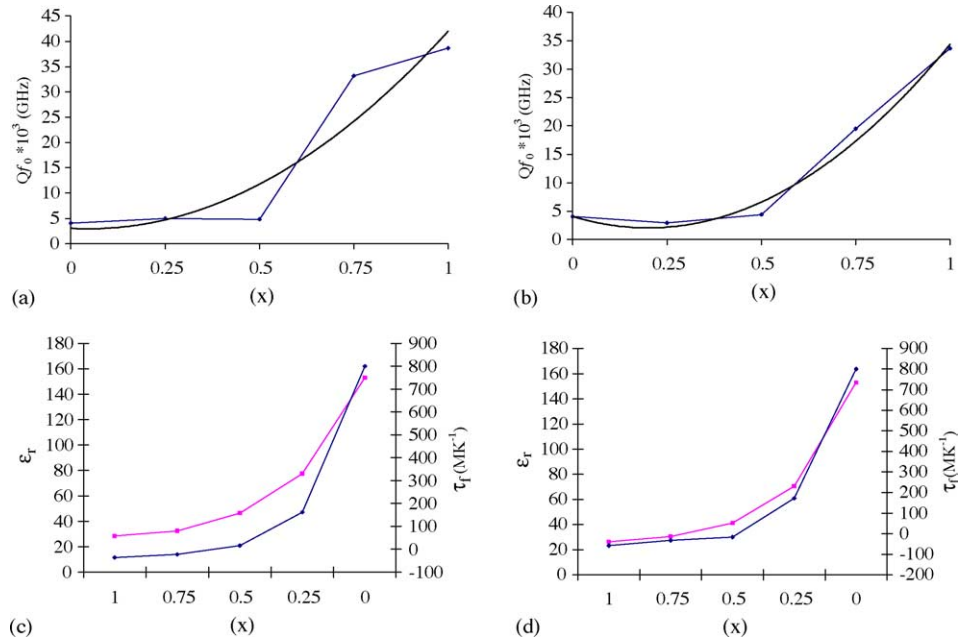

Fig. 6. (a) and (b) Qf_0 vs. x and (c) and (d) ε_r and τ_f vs. x for xLCT and xNCT.

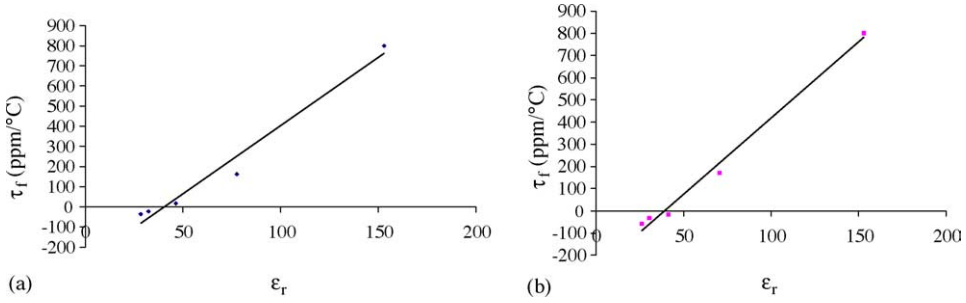

Fig. 7. ε_r vs. τ_f for (a) xLCT and (b) xNCT solid solutions.

4. Conclusions

- Dense (>95% theoretical), single phase ceramics were fabricated in the xLCT and xNCT solid solution series. XRD data revealed the presence of two anomalous peaks that were due to ZrO_2 contamination from the milling media.
- XRD and electron diffraction data suggested an $a^-a^-c^+$ tilt system for all compositions fabricated but XRD traces for LCT and NCT did not reveal any unique reflections of the type $\frac{1}{2}\{o\,o\,o\}_p$, $h=k=l$ associated with B-site ordering. However, electron diffraction patterns revealed $\frac{1}{2}\{o\,o\,o\}_p$ superlattice reflections in all pseudocubic $\langle 1\,1\,0\rangle_p$ directions for LCT and NCT consistent with of $P2_1/n$ (ordered) rather than *Pbnm* (disordered) symmetry. The absence of B-site ordered reflections in XRD traces for LCT and NCT is explained by the small scattering length difference between Ti^{4+} and Co^{2+}. For samples where $x<1$, the pseudocubic $\langle 1\,1\,0\rangle_p$ zone axes were consistent with *Pbnm* symmetry.
- LCT and NCT were highly insulating with Qf_0 values >30,000 GHz, $\varepsilon_r \sim 27$ and negative τ_f. As CT increased, ε_r increased, but Qf_0 decreased, possibly due to the loss of 1:1 long range, B-site order. For xLCT and xNCT, zero τ_f compositions are expected to occur at $x=0.48$ and 0.52 with $\varepsilon_r=45$ and 43 and $Qf_0 \sim 5000$ and ~4000, respectively.

Acknowledgements

The authors would like to thank Dr. P. Korgul and Mr. H. Bagshaw for help with electron microscopy. DLC would also lie to thank the Engineering and Physical Science Research Council for their continuing support.

References

1. Hirahara, S., Fujikawa, N., Enami, S. and Noshi, T., *Dielectric Ceramic Composition and Dielectric Resonator $Ln_2O_xAl_2O_3$–SrO–TiO_2*. U.S. patent no. 5356844, 1994.
2. Cho, S. Y., Kim, I. T. and Hong, K. S., Microwave dielectric properties and applications of rare-earth aluminates. *J. Mater. Res.*, 1999, **14**(1), 114–119.

3. Seabra, M. P., Salak, A. N., Avdeev, M. and Ferreira, V. M., Structure and dielectric characterisation of the $La(Mg_{1/2}Ti_{1/2})O_3$–$Nd(Mg_{1/2}Ti_{1/2})O_3$ systems. *J. Phys. Condens. Matter*, 2003, **15**(24), 4229–4238.
4. Glazer, A. M., Simple ways of determining perovskite structures. *Acta Crystallogr.*, 1975, **A31**, 756–762.
5. Seabra, M. P., Salak, A. N., Avdeev, M. and Ferreira, V. M., Structure and dielectric characterization of the $La(Mg_{1/2}Ti_{1/2})$O-3–$Nd(Mg_{1/2}Ti_{1/2})$O-3 system. *J. Phys. Condens. Matter*, 2003, **15**(24), 4229–4238.
6. Seabra, M. P., Avdeev, M., Ferreira, V. M., Pullar, R. C. and Alford, N. M., Structure and microwave dielectric properties of $La(Mg_{0.5}Ti_{0.5})$O-3–$CaTiO_3$ system. *J. Eur. Ceram. Soc.*, 2003, **23**(14), 2403–2408.
7. Avdeev, M., Seabra, M. P. and Ferreira, V. M., Structure evolution in $La(Mg_{0.5}Ti_{0.5})$O-3–$SrTiO_3$ system. *Mater. Res. Bull.*, 2002, **37**(8), 1459–1468.
8. Seabra, M. P., Avdeev, M., Ferreira, V. M., Pullar, R. C., Alford, N. M. and Reaney, I. M., Structure–property relations in xBaTiO(3)–$(1-x)La(Mg_{1/2}Ti_{1/2})$O-3 solid solutions. *J. Am. Ceram. Soc.*, 2004, **87**(4), 584–590.
9. Hughes, H., Iddles, D. M. and Reaney, I. M., Niobate-based microwave dielectrics suitable for third generation mobile phone base stations. *Appl. Phys. Lett.*, 2001, **79**(18), 2952–2954.
10. Reaney, I. M., Iqbal, I., Zheng, H., Feteira, A., Hughes, H., Iddles, D. *et al.*, Order–disorder behaviour in 0. $9Ba([Zn_{0.60}Co_{0.40}]_{1/3}Nb_{2/3})O_3$-$0.1Ba(Ga_{0.5}Ta_{0.5})O_3$ microwave dielectric resonators. *J. Eur. Ceram. Soc.*, 2005, **25**, 1183–1189.
11. Cairns, D. L., Reaney, I. M., Zheng, H., Iddles, D. and Price, T., Synthesis and characterisation of $La(Co_{1/2}Ti_{1/2})O_3$. *J. Eur. Ceram. Soc.*, 2005, **25**(4), 433–439.
12. Reaney, I. M., Colla, E. L. and Setter, N., Dielectric structural characteristics of Ba- and Sr-based complex perovskites as a function of tolerance factor. *Jpn. J. Appl. Phys.*, 1994, **33**(Part 1, 7A), 3984–3990.
13. Davies, P. K., Tong, J. Z. and Negas, T., Effect of ordering-induced domain boundaries on low-loss $Ba(Zn_{1/3}Ta_{2/3})$O-3–$BaZrO_3$ perovskite microwave dielectrics. *J. Am. Ceram. Soc.*, 1997, **80**(7), 1727–1740.
14. Harrop, P. J., Temperature coefficients of capacitance of solids. *J. Mater. Sci.*, 1969, **4**, 370–374.
15. Wise, P. L., Reaney, I. M., Lee, W. E., Iddles, D. M., Cannell, D. S. and Price, T. J., Tunability of tau(f) in perovskites and related compounds. *J. Mater. Res.*, 2002, **17**(8), 2033–2040.
16. Seabra, M. P., Avdeev, M., Ferreira, V. M., Pullar, R. C., Alford, N. M. and Reaney, I. M., Structure–property relations in xBaTiO(3)–$(1-x)La(Mg_{1/2}Ti_{1/2})$O-3 solid solutions. *J. Am. Ceram. Soc.*, 2004, **87**(4), 584–590.
17. Colla, E., Reaney, I. M. and Setter, N., Effect of structural-changes in complex perovskites on the temperature-coefficient of the relative permittivity. *J. Appl. Phys.*, 1993, **74**(5), 3414–3425.